Education and Culture DG

Erasmus Mundus

MODELLING OF PLASMA INTERACTION WITH CASTELLATED SURFACES IN FUSION DEVICES

Master Thesis
presented by

Michael Komm

Thesis promoters

Prof. Guido van Oost
Universiteit Gent

Prof. Gérard Bonhomme
Université Henri Poincaré

Prof. Michael Tendler
KTH Stockholm

Thesis supervisor

Dr. Andreas Kirschner
Institute of Energy Research – Plasma Physics
Association EUROATOM – FZJ

Erasmus Mundus Master on Nuclear Fusion Science and Engineering Physics

29.07.2009, Jülich

Contents

Copyright notice

Abstract

Nuclear fusion is a promising way to realize new clean source of energy with virtually unlimited amount of fuel. The International Thermonuclear Experimental Reactor (ITER) aims to demonstrate the feasibility of such goal. The proposed fusion reaction involves tritium, radioactive isotope of hydrogen. The amount of tritium inside the reactor chamber is restricted due to safety regulations. Experiments on existing devices indicate that tritium will have strong tendency to be accumulated inside the chamber. This predicts limitations of the reactor availability, which is highly undesirable. A substantial part of the fuel is accumulated in the castellated plasma facing components which are in particular difficult to access by cleaning techniques.

In order to understand the fuel retention mechanisms in gaps between castellated plasma facing components, an impurity transport code 3DGAP has been developed. The code used simplified model of particle flux coming from the plasma, while reaching only partial agreement with experimental results. The aim of the present work is to provide more realistic distribution of particle fluxes inside the poloidal gaps, both shaped and non-shaped, which can be calculated by a Particle-In-Cell code SPICE2. The behavior of plasma in the vicinity of the gaps is studied and important transport mechanisms identified. Impurity simulations with the improved model of plasma particle fluxes are performed and compared to the simple model. Also the role of ionization inside the gap is discussed.

The second part of the thesis is focused on fluid calculations of the SOL plasma in COMPASS tokamak by means of the B2SOLPS code. The results are compared to neoclassical calculations.

Chapter 1

Introduction

1.1 Fusion Energy

As the world population continues to grow and industry production increases, the question of suitable energy sources becomes more and more a topic of interest. The current main sources (coal, oil and nuclear fission) are all rather limited [1], although the estimates of their reserves vary widely. In addition, their resources are localized, which creates political dependencies and tensions between countries. For these reasons, there is an intensive ongoing research in the field of alternative energy sources.

One possibility are renewable sources, which usually include water, wind, solar, tidal and geothermal power stations. These sources do not require any fuel in the conventional meaning, however, their energy production is not stable but fluctuates with natural conditions. The problem of energy storage on a large scale is still unresolved, and so these sources are not suitable for industry and other applications, which require constant power supply.

A candidate for a source with abundant fuel and sufficient reserves for a long period of time is nuclear fusion. Unlike fission, where heavy nucleus is being split into lighter parts, which is accompanied by energy release, in fusion light nuclei are fused into a heavier one, which also produces a large amount of energy (of order 10^6 times more than in chemical reactions). Since all nuclei have positive charge, a strong force is needed to push nuclei close together, so that fusion can occur. In stars, this force is the gravitational force, here on Earth other approaches have to be studied. The most promising way to achieve fusion is to keep thermalized fusion fuel in the plasma state at high density for long enough time, so that collisions between plasma particles result in fusion. The suitable temperature of plasma is governed by the effective cross-section of each fusion reaction, the plasma density and critical

time is related by the *Lawson criterion*[2]. The reaction with highest reaction rate, which is currently intended to be used in the first generation of fusion reactors is the following:

$$D + T \rightarrow {}^4He + n + 17.59MeV. \tag{1.1}$$

The reactants here are isotopes of hydrogen - deuterium, which is stable and widespread in water, and tritium, which decays as a β emitter with half-time of 12.3 years. Tritium can be produced inside the plant by bombardment of a lithium blanket with the neutrons from fusion reactions. This is called tritium breeding

$$n + {}^6Li \rightarrow {}^4He + T + 4.8MeV \tag{1.2}$$
$$n + {}^7Li \rightarrow {}^4He + T + n - 2.5MeV. \tag{1.3}$$

Lithium can be extracted from soil. The estimates of resource reserves state that there is sufficient deuterium and lithium on Earth to cover at least 10^7 years of world energy consumption. The reaction does not require transportation of radioactive elements (tritium will be produced inside the plant) and does not produce direct radioactive waste. However, some parts of the reactor will get activated by fusion neutrons. This activation can be reduced by a choice of suitable materials and in total is much less problematic than in standard fission reactors. Unlike fission, there is no chain reaction involved and the conditions for fusion are extremely difficult to achieve and so the risk of uncontrolled reactions is negligible.

Tokamaks are presently considered to be the most advanced fusion approach, although several alternatives are being investigated. The largest current fusion device, JET (Joint European Torus), is of tokamak type and so will be the forecoming ITER (International Thermonuclear Experimental Reactor) machine [3]. The plasma in tokamak is magnetically confined in a toroidally shaped vacuum vessel. Schematic view of a tokamak device is shown in Fig. 1.1. The *toroidal* direction follows the center of the torus (and also the plasma current), while the *poloidal* direction wraps around the plasma cross-section. The toroidal magnetic field is produced by coils, while the poloidal field is created by the plasma current. This combined magnetic field reduces radial particle and energy losses and at the same time plasma current heats up the plasma. Tokamaks work as transformers, where the plasma serves as its secondary winding. The plasma current is driven by induction and as such, tokamaks were originally designed as short-pulsed devices with discharges lasting few seconds at maximum. Later, non-inductive

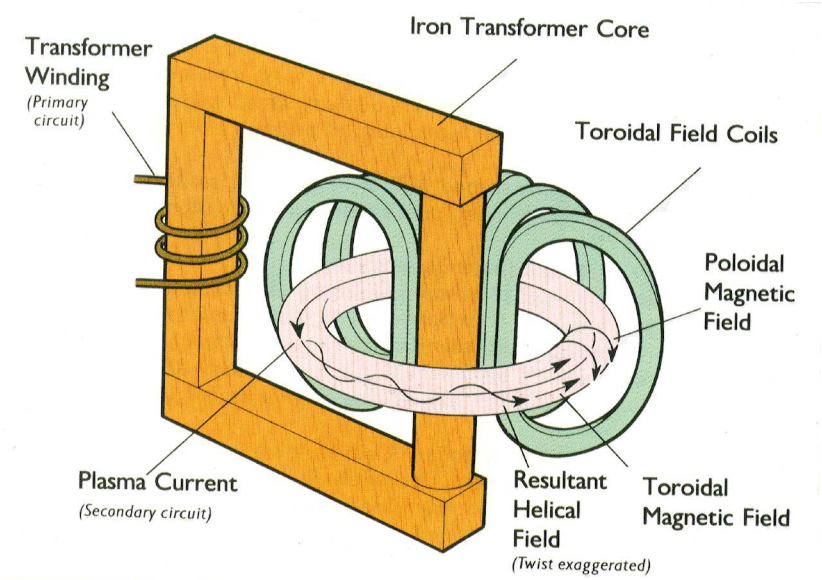

Figure 1.1: Main components and directions in tokamak.

means of current drive were discovered and today some tokamaks are capable of discharges several minutes long.

Tokamak dimensions can be briefly described by two main parameters - the major radius R (radius of the plasma loop) and minor radius a (radius of the plasma cross-section). The radii have been increasing throughout the history of fusion research, JET parameters are $R = 2.96$ m, $a = 2.10$ m and ITER will have $R = 6.2$ m and $a = 2.0$ m.

1.2 Fuel retention

Future fusion reactors will be using D-T mixture as a fuel. While the physical properties of deuterium are practically the same as of hydrogen, tritium is an unstable isotope, a weak β emitter with a half-time of 12.3 years. It behaves chemically in the same way as hydrogen, so it can be easily bound in water (HTO) or in various hydrocarbons. As such, it can easily penetrate into living organisms, increasing the destructive power of β radiation. The biological half-time of tritium in human body is roughly 10 days. There are several safety regulations concerning the manipulation with tritium to ensure the safe operation of the reactor. One of them restricts the amount of tritium that can be contained in the vacuum chamber. This limit reads approximately 1 kg of tritium for the ITER device. Given that the amount of tritium in

the plasma is supposed to be in order of grams it seems that this regulation will not bring any difficulties. However, a long term research has shown that the fuel has a very strong tendency to get accumulated in the walls of the vacuum vessel and in plasma facing components. So far, most of the fusion experiments have been done with deuterium but the unfortunate properties of tritium are expected to be similar. The fuel retention is a subject of intensive research, the mechanisms of deuterium/tritium accumulation are studied on many tokamaks, such as JET, TEXTOR, TORE SUPRA and DIII-D, or linear devices like PISCES. The amount of fuel retained in the vessel can be studied by different approaches - gas balance (to measure how much fuel is pumped out after discharge) or post-mortem material analysis of plasma-facing components (PFCs). This leads to rather wide range of estimated retention between 2 - 20% [4]. This amount depends mainly on the material of PFCs and its temperature during discharge. Measurements on DIII-D show that up to 40% [5] of retained fuel can be stored in gaps between castelated PFCs. More importantly, the gaps are particularly difficult for access by cleaning techniques, which help to reduce the fraction of fuel retained inside the vessel.

Each wall material has its own mechanisms of retention. Carbon is capable of chemical erosion and formation of deuterium-enabled hydrocarbons. These hydrocarbons can be deposited in layers and as such do not exhibit any saturation of retention. In case of beryllium and tungsten, chemical erosion does not occur and so the main mechanisms of accumulation is ion implantation and subsequent bulk diffusion. Co-deposition of fuel in layers is still observed in case of beryllium, as there is high sputtering followed by re-deposition. Overall, the level of accumulation is expected to be much lower than in case of carbon, which restricts its use in proposed reactors. Unfortunately, it is rather difficult to achieve high performance discharges in machines with tungsten walls, unless intensive boronization is used [6]. This has important consequences for ITER. In the tritium phase, ITER is planned to operate without carbon, only with a combination of beryllium and tungsten PFCs. However, in the first (hydrogen) phase, it will have CFC divertor tiles, which should facilitate initial experimental discharges. The predicted number of ITER discharges before reaching the safety limit of tritium retention for each material combination is shown in Fig. 1.2

1.3 Investigation of gaps

The physics of plasma behavior in the vicinity of tile gaps is an complicated issue, which is a subject of intensive research on a number of machines.

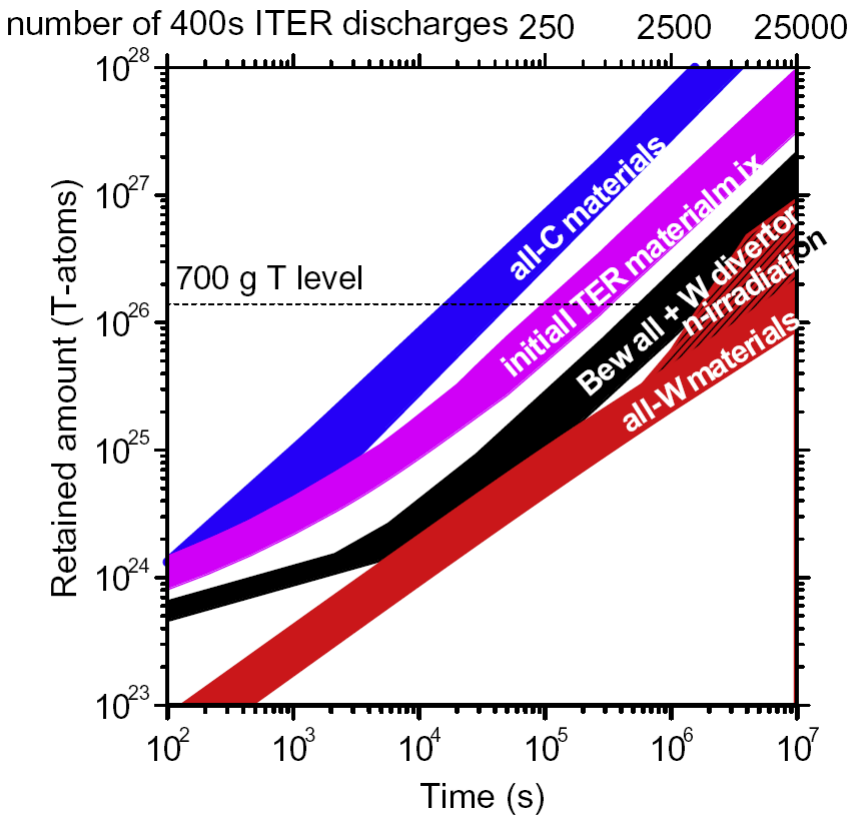

Figure 1.2: Estimated number of allowed ITER discharges for different material combinations [7].

There has been a dedicated experiment [8] at the TEXTOR tokamak with so-called test limiter to study deposition inside gaps of castellated surfaces. The geometry of the limiter is shown in Fig.1.3. This limiter consisted of both shaped and non-shaped gaps 0.5 mm wide between rectangular tiles of 10 mm. After a sequence of discharges, the test limiter was removed from TEXTOR and analyzed. Results from the post-mortem analysis provide information about the material mixing, erosion and deposition [9] inside gaps but no direct observations of the transport mechanisms. Theoretical modeling of the gaps involves estimation of a number of unknown parameters, which results in only partial agreement with experiment. The aim of this work is to improve the theoretical model 3DGAP previously developed at Forschungszentrum Jülich [10] in order to study layer formation inside the gaps by providing a realistic plasma particle flux and electrical potential distribution. These characteristics are calculated by a 2D Particle-In-Cell code SPICE2 [11], which is described in more detail in chapter 3.

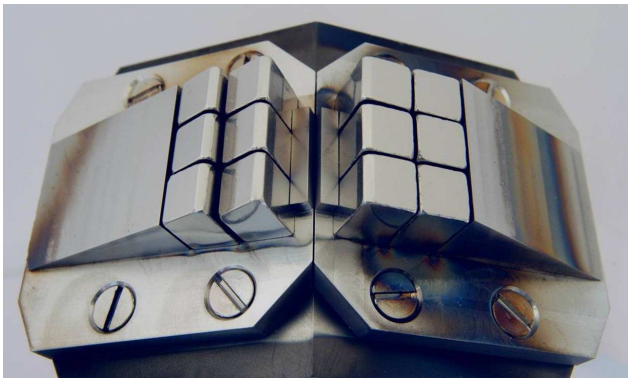

Figure 1.3: Photo of the TEXTOR test limiter with shaped and non-shaped gaps.

Chapter 2

Theory

2.1 Edge plasma physics

2.1.1 Plasma-wall interaction

As described in previous chapter, in order to achieve conditions suitable for fusion, it is necessary to keep plasma at very high temperatures and well separated from the walls of the vacuum vessel. Any contact of hot plasma with the solid material leads to destructive processes - energetic ions hitting the surface cause physical sputtering, some can induce chemical reactions resulting in additional chemical erosion. Should the heat load be too high, melting and droplet formation can occur on metallic surfaces. Eroded material can be deposited on other parts of surface either by implantation or layer formation. Impurities in plasma can work as a energy loss channel via cyclic ionization and recombination. Even the sophisticated toroidal configuration with twisted magnetic field lines does not result in perfect confinement - processes like collisions or various instabilities create a cross-field transport towards the walls of the system [12]. It is therefore necessary to form special parts of the vessel, which will withstand the contact with the plasma and minimize the negative effects described above.

2.1.2 Plasma sheath

In order to understand the plasma-surface interactions it is necessary to study the plasma behavior in the vicinity of the surface. In general, electrons have higher mobility than ions so their charge flow towards a solid material with plasma would dominate that of ions. This is the reason why all objects in plasma saturate with negative charge (supposing there is no biasing). This charge creates a drop of the plasma potential, called the *sheath*. In

equilibrium, the sheath repulses electrons and attracts ions towards the wall so that the net current is zero. The sheath has a typical thickness of several Debye lengths [2] (few tenths of millimeters in tokamaks) and only a small part of the potential drop (~ 0.7 kT$_e$) called *presheath* extends further into the plasma. The potential drop across the sheath can be calculated from a simple 1D model with monoenergetic ions and Boltzmann electrons [2] and the resulting formula is as follows:

$$-\frac{e\phi_0}{T_e} = \frac{1}{2} ln \left[\frac{(1-\delta^2)m_i/m_e}{2\pi(1+T_i/T_e)} \right]. \tag{2.1}$$

where m_i and m_e are ion and electron masses respectively, and δ is the coefficient of secondary emission. The logarithmic expression is not very sensitive to small changes in temperature ratios, the potential drop has a value around 3 kT$_e$ for typical edge plasma parameters. The coefficient δ can be close to unity and so the secondary emission can significantly affect the sheath. The plasma in sheath follows the *Bohm criterion* [2], which states that ions enter the sheath at their sound speed.

2.1.3 Chodura sheath

Simple model of the sheath described above was premising absence of the magnetic field or a homogeneous magnetic field perpendicular to the surface (and so without any effect on the model). However, all fusion devices operate under a strong magnetic field and the field lines have usually an oblique angle of a few degrees with respect to the surface. The reason for this is an engineering issue - for envisaged reactor target plasma the parallel heat load would be of order 10^8 Wm^{-2} - 2 orders of magnitude beyond the material safety limits. It is therefore necessary to spread the load over a larger surface.

The electric properties of plasma can be characterized by a length parameter - the Debye length λ_D. The presence of magnetic field brings about another important parameter - the Larmor radius r_l. The ratio of these paramaters

$$\xi = \frac{\lambda_D}{r_l} \tag{2.2}$$

determines the nature of the magnetic sheath - the *Chodura sheath* [13]. For typical tokamak SOL plasma (n $= 10^{19}$ m^{-3}, T$_e = 20$ eV), the Debye length is of the order of 10^{-5}m, while the ion Larmor radius is usually few millimeters. In order to understand the particle motion in the magnetic sheath, we shall start with a simple model of a homogeneous B field in the z axis direction and perpendicular, constant gradient of E field in y axis direction (in the

direction towards the surface). In reality the gradient of the sheath E field varies approximately exponentially towards the surface but the consequences are similar. The equation of motion reads

$$\frac{d\mathbf{v}}{dt} = \frac{q}{m}\left[\mathbf{E} + (\mathbf{v} \times \mathbf{B})\right] \tag{2.3}$$

Here we put $B_z = B$, other components are zero and $E_y = E_0 + ay$ is a linearly increasing field. The solution of this set of coupled differential equations is the following:

$$\frac{d^2 v_z}{dt^2} = \frac{q}{m}\left[a - \frac{q}{m}B^2\right] v_y, \tag{2.4}$$

and an important limiting condition

$$a > \frac{q}{m}B^2 \tag{2.5}$$

This equation has two types of solutions, for $a < \frac{q}{m}B^2$ it is the standard oscillatory Larmor motion (though with modified gyro-frequency). For $a > \frac{q}{m}B^2$ the solution is exponential, the classical motion breaks. This is called *demagnetization*. Inside the sheath the gradient of electric field (here represented by a) can easily exceed this limit and so ξ should be smaller than one, the effects of magnetic field will be drowned out by the electrical sheath. However, in the typical tokamak SOL plasma, ξ has typical values 10 - 50. In this case new region called *magnetic pre-sheath* appears. Situated between the sheath and the plasma, this region is approximately quasineutral but the plasma density decreases. The graphs 2.1 show important features of the magnetic sheath - the Bohm criterion is still fulfilled and ions enter the sheath at their sound speeds.

2.2 Introduction to plasma modeling

This section gives very brief introduction into various approaches used in numerical simulations of plasma. Numerical models have been used in plasma research for decades and resulted in a large family of different methods; here only the most important ones are discussed.

2.2.1 Fluid modeling

Given the complicated behavior of hot plasma, it is almost suprising how many situations can be modeled using a simple fluid approximation. These models do no take into account the particle-related properties of plasma but

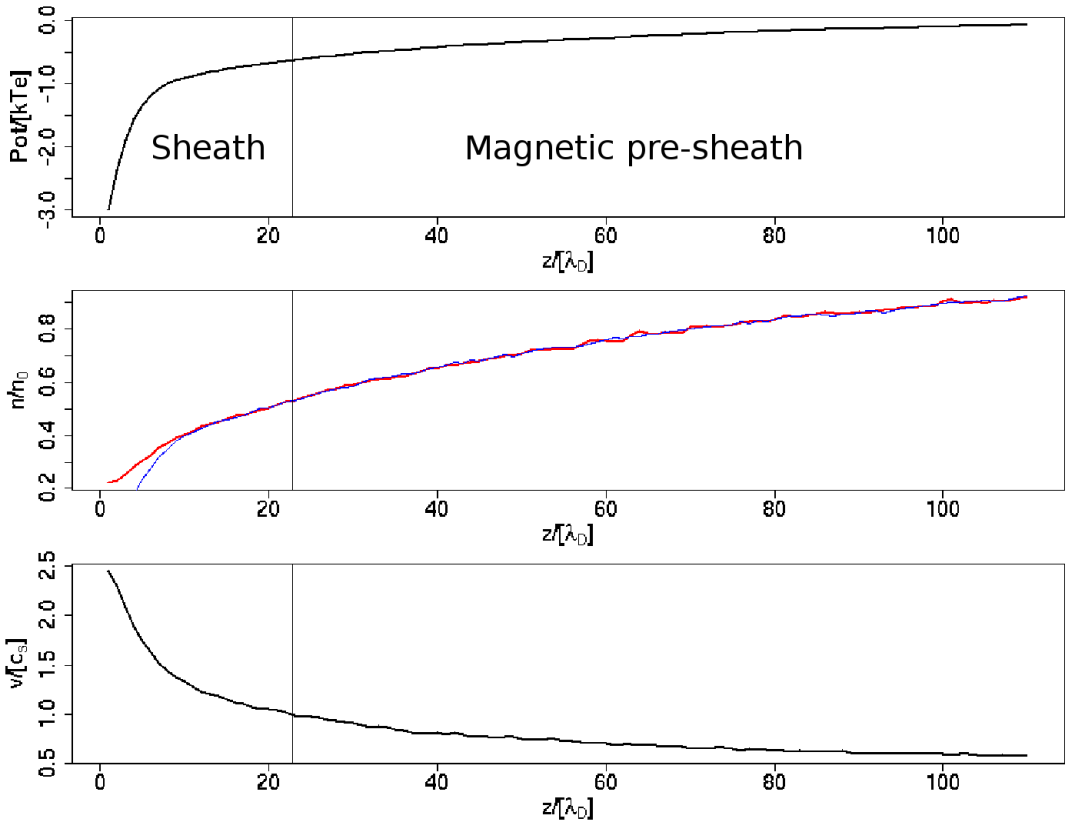

Figure 2.1: Density and potential drop in the magnetic sheath (red ion density, blue electrons), third graph shows increase of the ion speed.

assuming a Maxwellian distribution regarding the plasma as a fluid, continuous quantity. The modeling consists of simultaneous solution of equations relating plasma density, temperature, pressure and electric field. In general, the fluid models (especially those with reduced dimensions) are very fast and allow to model huge volumes of plasma. The main inconvenience is the assumption of quasineutrality and Maxwellian distribution of particle velocities, which are not satisfied in the sheath. That is why fluid models are not suitable for modeling of the sheath. An example of fluid code is widely used B2SOLPS [14], which is describe more in detail in chapter 5.

2.2.2 Vlasov equation modeling

Vlasov (or Fokker-Planck) equation is the basic relation of kinetic theory of plasma. The equation reads

$$\frac{\partial f}{\partial t} + \mathbf{v} \cdot \nabla f + \frac{q}{m} \left(\mathbf{E} + \mathbf{v} \times \mathbf{B} \right) . \frac{\partial f}{\partial \mathbf{v}} = \left[\frac{\delta f}{\delta t} \right]_s . \tag{2.6}$$

The solution of this equation is a distribution function varying in time and space. The knowledge of the distribution function allows calculation of the fluid quantities by simple integration

$$n = \int_{-\infty}^{\infty} f(v) dv, \tag{2.7}$$

$$\Gamma = \int_{-\infty}^{\infty} v f(v) dv, \tag{2.8}$$

etc. The term on the right hand side of eq. 2.6 is the collisional term, which can take many forms depending on the situation. The Vlasov modeling gives more detailed information about plasma behavior and does not have any Maxwellian assumption but still ignores individual particles. The models to solve this equation are in general much slower than fluid models and rather complicated.

2.2.3 Particle-In-Cell modeling

Particle-In-Cell [15] modeling represents the most detailed way of plasma modeling. The trajectory of every particle is being calculated from its equation of motion

$$\frac{dv_i}{dt} = \frac{q_i}{m_i} \left(\mathbf{E} + \mathbf{v}_i \times \mathbf{B} \right) . \tag{2.9}$$

In most cases, the magnetic field is externally imposed and the electric field is calculated using the Poisson equation

$$\triangle\phi = -\frac{\rho}{\epsilon_0}, \tag{2.10}$$

$$\mathbf{E} = -\nabla\phi. \tag{2.11}$$

A truly kinetic calculation of fusion plasma would be impossible to perform on present hardware - with typical plasma density of 10^{19} m^{-3}, the model would have to follow 10^{13} particles just to simulate one cubic centimeter of plasma. Therefore a number of speed-up tricks is being used to make the simulation possible while keeping the physical reliability. Instead of calculating the path of every single particle, it is common to calculate the movement of clouds of particles, so called *macroparticles* The typical number of particles contained in one macroparticle is of the order of $10^6 - 10^7$. In most cases this simplification does not cause any constrains. However, for certain problems (e.g. simulation of a very small plasma current flowing to a surface) artificial oscillations can occur.

Kinetic codes take often benefit of spatial symmetry to reduce the number of dimensions. The speed-up is significant - 1D simulation of a typical plasma sheath can take some tens of minutes, 2D simulation few days and a full 3D simulation requires high computing power, usually in a parallelized environment. The 2D kinetic codes are becoming a standard tool on present hardware for probe calibration or plasma sheath modeling, 3D codes are still highly experimental.

In order to calculate the precise electric force acting on a particle in plasma, it is necessary to take into account interaction between every pair of particles

$$F_i = \sum_{j=1}^{n} F_{ij} = \frac{q_i}{4\pi\epsilon_0} \sum_{j=1}^{n} \frac{q_j}{r_{ij}^2}. \tag{2.12}$$

The time dependence of any such algorithm corresponds to $\sim n^2$ in the best case. To improve this dependence, the space region is divided by a grid, charge density is being calculated on every grid node and then using Poisson equation discrete potential is obtained. This simplification is called *Particle-in-Cell* (PIC). PIC codes have time dependence $\sim n \log n$. The discretization brings the following requirements to ensure correctness of calculations.

- The number of macroparticles in one cell should not be less than 50
- The size of the cell should not exceed the Debye length

- Particle should not cross a whole cell during one timestep.

These are very general conditions, which can in fact vary depending on the actual situation. PIC codes are precise when calculating regions, where quasineutrality is not satisfied. However, in the quasineutral regions (with charge density close to zero) they tend to exhibit numerical fluctuations of electric potential. It is therefore profitable to model quasineutral regions (ie. the presheath) by fluid codes and the small sheath area by a PIC code.

Despite all listed enhancements, the computational demand of kinetic codes is still an important issue. Much progress has been recently done in discovering new fast methods of solving the Poisson equation (traditionally the most demanding part of the code) and in parallelization of the codes.

2.2.4 Gyro-kinetic modeling

This modeling approach also deals with single particles but uses the guiding-center approach. This allows to increase significantly the timestep - in traditional kinetic codes the timestep should not exceed the electron gyro-rotation period. Such enhancement is not very suitable for cases where guiding center motion is not being preserved (ie. the sheath). However, this approach allows precise simulations of SOL with non-Maxwellian distributions - for example due to heating or current drive. An example of a gyro-kinetic code is Gysela 5D [16], which simulates the whole Tore Supra tokamak in 5 dimensions. A simulation on a supercomputer with 1000 processors is estimated to take about 72 hours, which illustrates the computing demands of these codes.

Chapter 3

SPICE2 code

This chapter provides detailed description of the SPICE2 (**S**heath **P**article **I**n **CE**ll) code [17][18]. The development of the SPICE code has started in 2004 by Dr. R. Dejarnac (Institute of Plasma Physics, AS CR) and Dr. J.P. Gunn (CEA Cadarache, France). The code was originally one-dimensional with subsequent upgrade to two spatial dimensions. In July 2006 the code was fully functional but its performance was insufficient for realistic simulations. The first step to accelerate the code was done with help of Mgr. Z. Pekarek (FPP, MFF-UK, Prague) by implementing the fast direct Poisson solver. Further development of the code was then continued in the framework of this thesis.

The brief characterization of the code is:

- 2D in space, 3D in velocity
- Cartesian coordinates
- Dimensionless normalization
- Homogeneous magnetic field with variable inclination towards the surface
- Fast direct Poisson solver
- Injection of particles respecting the orientation of the magnetic field
- Variable geometry with arbitrary number of rectangular, triangular and circular objects
- Parallelization by groups of particles
- Binary output in Matlab format

3.1 Programming environment

The code is written in Fortran 90 and has been successfully compiled by the Intel, PGI and PathScale compiler on both 32 and 64 bit UNIX systems. The output of the code is stored in Matlab v4 binary files, which makes Matlab recommended software for data post-processing. However, the binary format is supported by many other visualization software.

3.2 Normalization

The code uses dimensionless normalization, which scales physical quantities by its typical values. The main advantage of the normalization is the reduction of the number of parameters defining one simulation and so the results of one dimensionless simulation can be de-normalized to a whole set of MKS scenarios. The normalization reads:

$$t \longrightarrow t \cdot \omega_i \tag{3.1}$$
$$x \longrightarrow x/\lambda_D \tag{3.2}$$
$$v \longrightarrow v/c_s \tag{3.3}$$
$$\phi \longrightarrow \phi\frac{kT_e}{e} \tag{3.4}$$
$$m \longrightarrow m/m_i \tag{3.5}$$
$$q \longrightarrow q/q_i \tag{3.6}$$
$$n \longrightarrow n/n_0 \tag{3.7}$$

where ω_i is the ion gyro-frequency, $c_s = \sqrt{kT_e/m_i}$ ion sound speed and n_0 the plasma density at sheath entrance. The code is using two important dimensionless parameters:

$$\xi = \frac{r_l}{\lambda_D} \tag{3.8}$$
$$\tau = T_i/T_e \tag{3.9}$$

The parameter ξ is the ratio of the ion Larmor radius and the Debye length, describing the relation between magnetic and electric sheath. The parameter τ is the ratio of the ion and electron temperature.

3.3 Particle injection

A correct injection of particles is a key point in a realistic plasma simulation. The simplest way of injecting particles from *unperturbed* plasma is to generate their velocities from Maxwellian distributions in all three dimensions. This commonly used technique disregards two important factors: effects of the presheath and presence of the magnetic field.

The SPICE2 code implements more sophisticated approach. The distribution function of $v_{||}$ is taken from a quasineutral code *QPIC* [19] (1D code that simulates the whole presheath) or *SOL1D* (1D code that simulates the Scrape-off layer). Due to the normalization, the only parameter that affects this distribution is τ, which is kept in most cases equal to unity. $f(v_{\perp_1})$ and $f(v_{\perp_2})$ are still Maxwellian. In real plasma such distributions are expected as well as the uniform distribution of the phase of Larmor gyration. This has to be kept in mind when transforming from the B field oriented velocities ($v_{||}$,$v_{\perp_1}$ and $v_{\perp_2}$) to cartesian velocities. The transformation is as follows

$$v_z = v_{||} b_z + v_{\perp_2} \sqrt{b_x^2 + b_y^2} \tag{3.10}$$

$$v_y = v_{||} b_y + \left(v_{\perp_1} b_x - v_{\perp_2} b_y b_z\right) / \sqrt{b_x^2 + b_y^2} \tag{3.11}$$

$$v_x = v_{||} b_x - \left(v_{\perp_1} b_y + v_{\perp_2} b_x b_z\right) / \sqrt{b_x^2 + b_y^2}, \tag{3.12}$$

$$\tag{3.13}$$

where b_x, b_y and b_z are directional cosines of the magnetic field. This setup generates uniform phase distribution and so avoids density cusps.

When generating the initial particle positions, one has to take into account the orientation of the magnetic field. Assuming zero electric field, particles in homogeneous B field follow a sine curve (in 2D). Apparently, this curve can have many intersections with the injection plane. With the standard boundary scenario (when particle leaves the simulation box, it is discarded) one would need to place the particle in the position of its last intersection with the injection plane. This leads to an artificial magnetic sheath formation near the injection plane (there are *missing* particles from the previous entrances of particles in the simulation box), which can significantly modify the particle velocity phase-space. The SPICE2 code handles this issue by adding an injection box with length of several ion r_L with zero electric field and injecting particles inside this box. This approach allows proper particle injection, however slows down the calculations (the code has to calculate the movements of particles in the injection box, which do not contribute to the simulation). This problem is a subject of future develop-

ment. The y position is chosen from a uniform distribution function, the z coordinate from the following formula

$$z = z_{mid} + v_{||} dt R b_z + q v_{\perp_1} m \sqrt{b_x^2 + b_y^2}, \tag{3.14}$$

where R is a random number between 0 and dt, the simulation timestep and q and m particle charge and mass. The random term is necessary to avoid artificial modes of the simulation.

3.4 Equation of motion

The SPICE2 code implements standard Leapfrog method [20] for particle advancing. The timestep is selected by two empiric criteria: electron should not move through a whole cell during one timestep and the timestep should be less then 1/10 of electron gyro-period

$$t_{crit_1} = \frac{1}{2} \frac{\sqrt{\frac{dz^2+dy^2}{\mu}}}{\xi} \tag{3.15}$$

$$t_{crit_2} = \frac{2\pi}{10\sqrt{\mu}}, \tag{3.16}$$

where μ is the ion-electron mass ratio, dz and dy cell dimensions. In most of the simulations $\mu = 200$ is used (instead of real $\mu = 3670$ for deuterium plasma), which allows increasing the timestep with a negligible impact on the results of the simulation. In future, the gyro-kinetic method for electrons will be implemented. This will allow further timestep increase.

3.5 Poisson solver

Solving the Poisson equation and thus obtaining the matrix of the electric field is a fundamental part of every PIC code. In most codes this also represents the part with highest computational demands. SPICE2 implements two different Poisson solvers - the iterative Gauss-Seidel method and direct LU decomposition method [21]. While the iterative solver takes typically 90% of the timestep time, the direct solver consumes only 5%. This allows parallelization of the code by particle groups.

Since the iterative Gauss-Seidel method is well-known standard method, here only the direct method is described. The normalized Poisson equation reads

$$\triangle \phi = -\rho. \tag{3.17}$$

Choosing uniform rectangular grid for discretization of the simulation box

$$y = h_y i \tag{3.18}$$
$$z = h_z j \tag{3.19}$$

The discrete Poisson equation now reads

$$\frac{\phi(i-1,j) - 2\phi(i,j) + \phi(i+1,j)}{h_z} + \frac{\phi(i,j-1) - 2\phi(i,j) + \phi(i,j+1)}{h_y} = -\rho(i,j). \tag{3.20}$$

Potential and charge density matrix are turned into a vector by putting the matrix lines one after another. For this a new index is introduced

$$k = i + jN_z. \tag{3.21}$$

To keep the explanation illustrative square cells are assumed. We can now rewrite the discrete Poisson equation as

$$\phi_{k+N} + \phi_{k+1} - 4\phi_k + \phi_{k-1} + \phi_{k-N} = -\rho_k h^2 \tag{3.22}$$

The Laplace operator in Poisson equation is transformed into a matrix. This matrix will have $m \times m$ cells, where m is $N_z \times N_y$. This means that the size of the matrix will grow as N^4, while most of the members will be zero. To avoid immense memory requirements, the *sparse matrix* format is used. This is achieved using the UMFPACK library [22]. To solve the Poisson equation, Laplace matrix is inverted (at the beginning of the simulation) and then every time multiplied with the vector of the charge density in order to obtain the potential

$$\phi = -\triangle^{-1}\rho. \tag{3.23}$$

This approach has a number of advantages - in general it is much faster than the iterative solvers, and the calculation of the potential has constant computational demands. Limitations of the method come at the first step - there has to be enough memory for the matrix inversion. The inversion itself is done by the LU decomposition by the GotoBLAS [23] library. A matrix of the grid 6000x2000 cells has been successfully inverted, which is far beyond the usual grid size (500x400).

3.6 Boundary Conditions

Figure 3.1 shows schematically the boundaries in present code geometry. The top boundary is fixed, we impose zero potential (unperturbed plasma). There

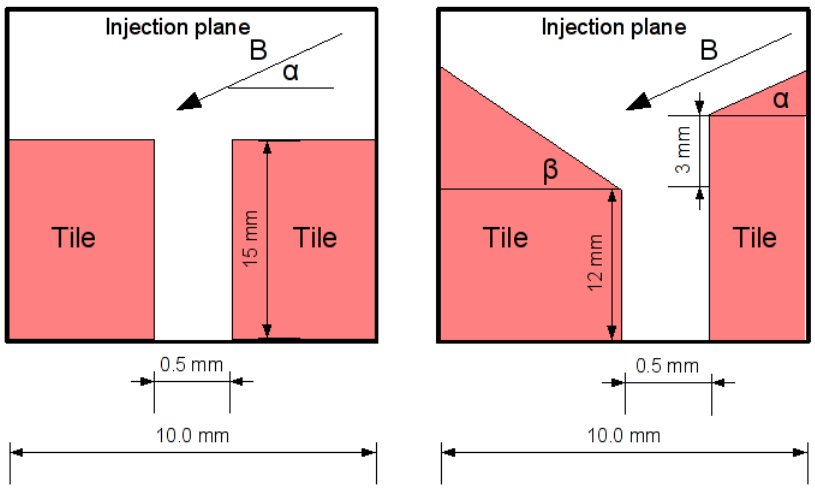

Figure 3.1: Geometry of the shaped and non-shaped gap.

is the injection box above the top boundary, so particles are being discarded only if they reach the top boundary of the injection box. Side boundaries are periodic, particles crossing them are being shifted by L_y or $-L_y$, respectively. The bottom boundary is again fixed, with the same imposed potential as the potential of the tiles, particles are being discarded when they reach it. The tiles are equipotential boundaries. The coordinate system is cartesian, with y direction parallel to the injection plane and z direction parallel to the gap.

3.7 Parallelization

The SPICE2 code is parallelized using the OpenMPI library [24]. In theory it allows to run on 99 parallel threads, however various practical constrains limit this number to some 40 - 60 threads. The parallelization is done by groups of particles (each processor has a certain number of particles) unlike the usual domain decomposition (each processor takes care of a part of the simulation box). This parallelization is possible only due to the fast Poisson solver, which takes only about $2 - 5\%$ of the iteration time. All remaining parts of the code can be calculated separately. This approach minimizes network traffic, which would otherwise be linked to particles crossing domain borders. The workflow of the code is schematically described in picture 3.2. The only traffic related to the parallelization is the transfer of charge densities calculated by each thread and then the distribution of the actual potential.

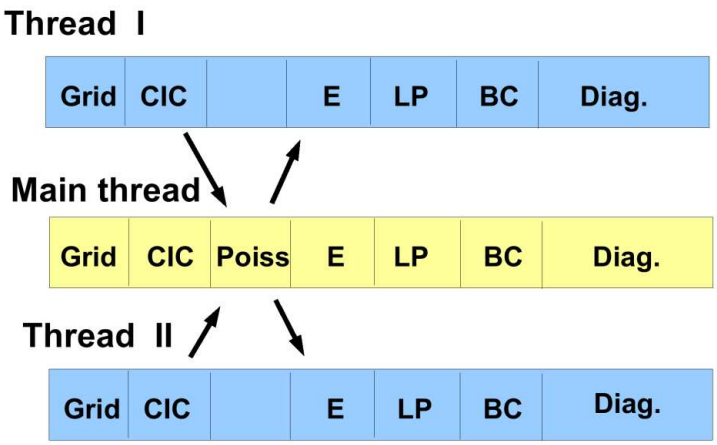

Figure 3.2: Workflow of the SPICE code.

3.8 I/O files

The SPICE2 code uses concept of the input file, which allows to run multiple simulations without compiling the code for each scenario. The input file is a simple text file and it allows to set all simulation parameters. For precise documentation of the input file format, see the code documentation [25].

The code produces three types of output files, all of them in Matlab v4 format. One output file (specified with the -t flag) stores all optional diagnostics, time histories, actual charge density and potential. This file is being produced every N steps (defined in the input file). Another file (defined by the -o flag) stores time-averaged diagnostics from the steady state regime. It is being saved every N steps once the simulation reaches the steady state. The last set of files stores the positions and velocities of particles. Such file is produced for every processor. This method is designed to minimize network traffic - files with particle positions are typically rather memory-consuming and rarely needed. The separation of time histories from time-averaged diagnostics simplifies post-processing. The code allows two ways of relaunching a simulation. First is so-called *continue* mode, where the code resumes particle positions, time histories and time-averaged diagnostics - it is designed for incidents when the simulation was aborted. Second is *restore* mode, where the particle positions are restored and time is set to the beginning of steady state. This mode allows modification of the input file (i.e. different diagnostics).

Chapter 4

Gap simulations

4.1 SPICE2 simulations

4.1.1 Introduction

Within the first part of the thesis work the plasma flux in the vicinity of TEXTOR test limiter tile gaps is simulated by means of the SPICE2 code. The gaps are either shaped or non-shaped (see Fig. 4.1). The setup of the simulations for non-shaped gaps is the following: rectangular cartesian simulation box, the top boundary is the plane of injection with fixed potential equal to zero, left and right boundaries are periodical. Two equipotential rectangular blocks represent the tiles with the gap in between them. The tiles are biased at floating potential ($V_{fl} = -3$ kT$_e$). The magnetic field is uniform with variable inclination with respect to the surface. This scenario, in fact, simulates an infinite set of parallel gaps. The distance between the injection plane and the tiles has to be sufficient to include the sheath and magnetic pre-sheath. Usually this distance has been put equal to 8 - 10 ξ, which is a well-tested empirical rule.

Two kinds of gaps are of interest: B field parallel (*toroidal*) or perpendicular to the gap (*poloidal*). The PIC simulations assume constant plasma conditions on the upper boundary. This is realistic in the case of poloidal gaps, however in toroidal gaps the radial position of gap entrance can vary and so do the plasma conditions. For this reason, this work will focus on poloidal gaps.

First a *standard* case has been defined, with typical plasma conditions of the TEXTOR tokamak. These conditions in the SOL are:

- Plasma density $n = 6 \times 10^{18}$ m^{-3}
- Ion temperature $T_i = 60$ eV

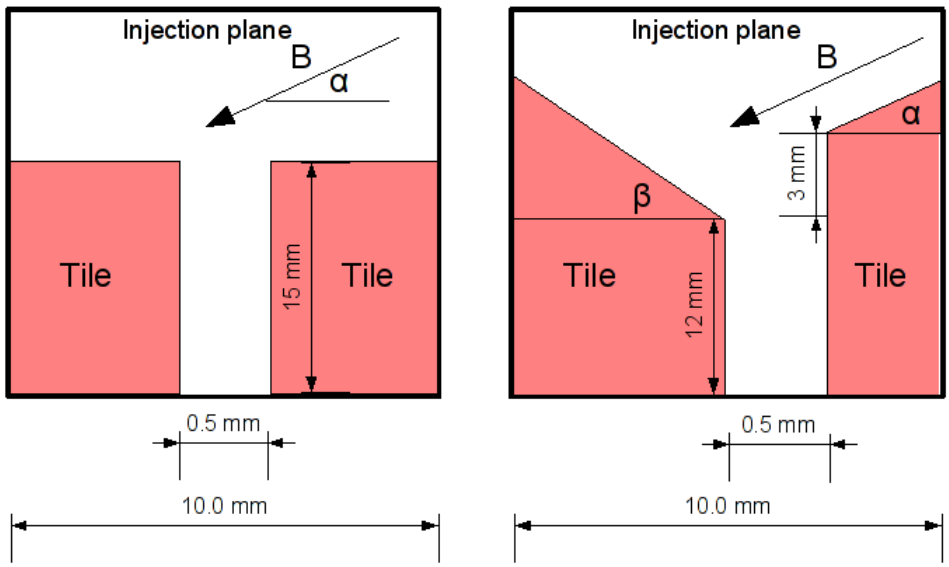

Figure 4.1: Geometry of the gap simulations.

- Electron temperature $T_e = 30$ eV
- Magnetic field magnitude $B = 2.25$ T
- Magnetic field inclination to tile surface $\alpha = 20°$
- Gap width $L_{gap} = 0.5$ mm

The physical processes can be best described on the electric potential distribution as shown on Fig. 4.2. Deuterium ions have Larmor radii comparable to the size of the gap and so they can penetrate inside the shadowed region. Electrons simply follow the field lines, as there is no mechanism of cross-field transport. This finite-Larmor effect results in net positive space charge inside the gap and subsequent formation of potential structure. The potential hill is positive and so repels more ions from entering the shadowed region. Some of these ions hit the gap in the plasma-wetted area, some are completely bounced off the gap and reach the top surface of the tile.

The deuterium ion flux distributions along the gap are shown in Fig. 4.3. The left tile, which is opened to direct plasma load, shows a complex decay structure. Near the entrance, there is a plateau region, which is governed by the potential structure, and further inside the gap there is exponential decay given by geometry of the gap. The right tile, which is in the plasma

shadow is also experiencing particle flux, altough it seems to be in contrary with simple geometrical ballistic model. The ion streamlines on Fig. 4.2 reveal that this is due to strong electric fields in the sheath - strong enough to attract ions, which would otherwise hit the left tile. The distribution of particle fluxes shows that typically 5% of particles coming from the plasma reach the right tile, 75% the left tile and 20% are bounced off the gap.

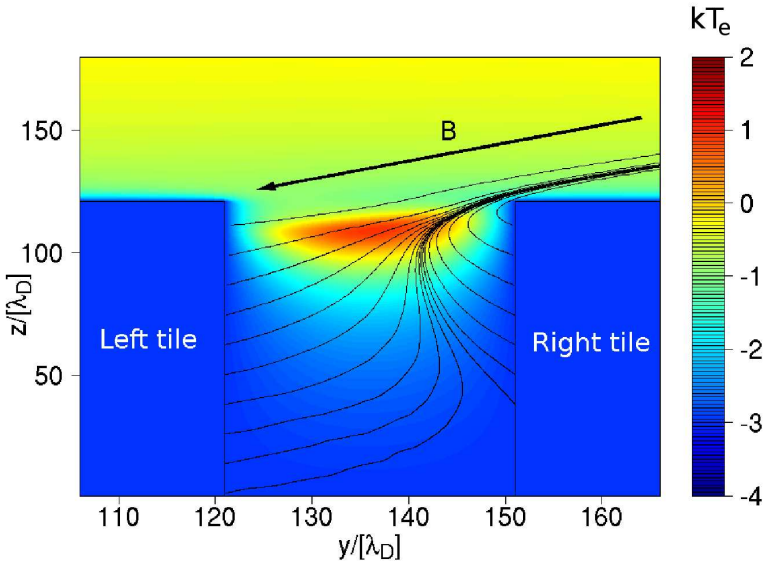

Figure 4.2: Potential profile of the standard case. Black lines represent ion streamlines.

4.1.2 Parameter study

In order to provide particle flux data for typical TEXTOR conditions, a set of simulations with varying plasma parameters was performed. The plasma density at the sheath entrance was studied in the range between 2×10^{18} and 1×10^{19} m^{-3} and the temperature between 40 - 100 eV. As shown in the standard case, the crucial parameter governing the particle fluxes along the gap is the potential structure near the entrance of the gap. The height of this potential hill (meaning the maximum of potential) for all the studied cases is summarized in Fig. 4.4. The contour lines for maximum potential of 0.5, 0.0 and -0.5 respectively separate the zones with different influence of the potential structure on the transport inside the gap.

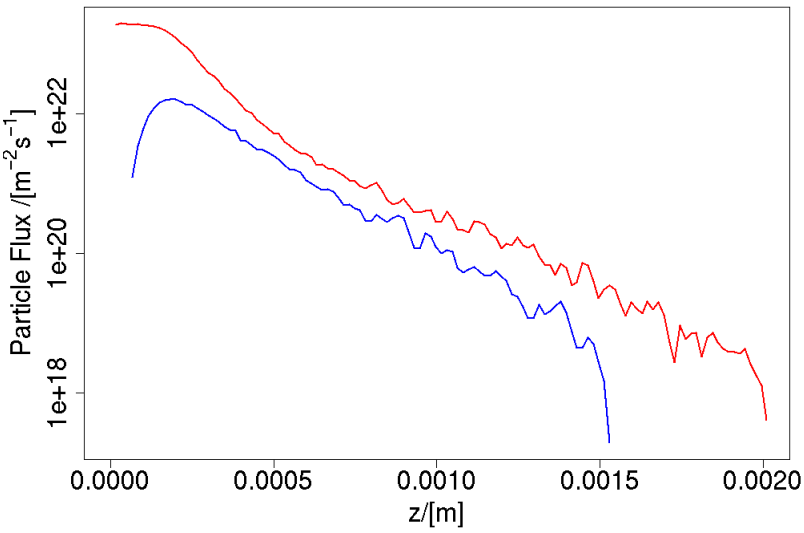

Figure 4.3: Deuterium flux distributions along the gap. Red curve represents the left tile, blue curve the right tile.

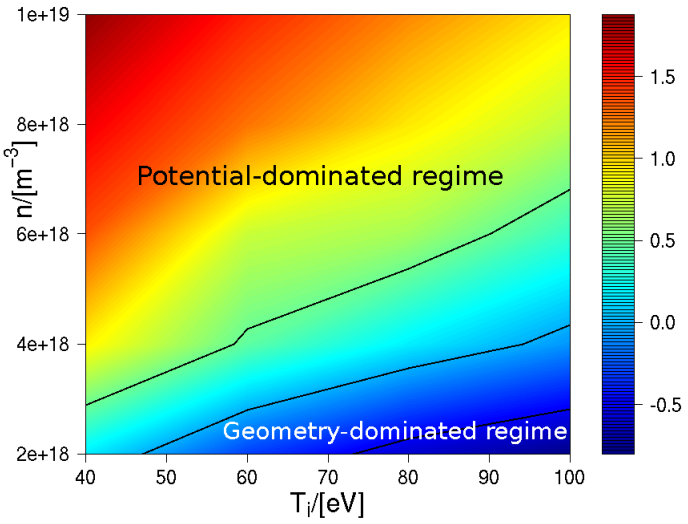

Figure 4.4: Maximum of potential at the potential hill inside the gap. Contour lines separate the zones of strong and weak influence of the hill.

One would expect, that the height of the structure is directly related to the penetration of ions into the gap and therefore a function of the ratio of ion Larmor radius to the gap width. It turns out that the height is much better modeled by a function

$$\phi_{max} = Ae^{\sqrt{\lambda_D}} + B \tag{4.1}$$

as shown in Fig. 4.5. The reason for this is that while the Larmor radius changes within the studied range of parameters only twice (0.28 - 0.45 mm), the Debye length, which is related to Poisson equation and thus to the potential response to a given charge density, changes almost 4 times (1.1 - 3.7 $\times 10^{-5}$ m). The fraction of gap width which is occupied by sheath (strong variation of potential) varies from negligible 6% to substantial 24%.

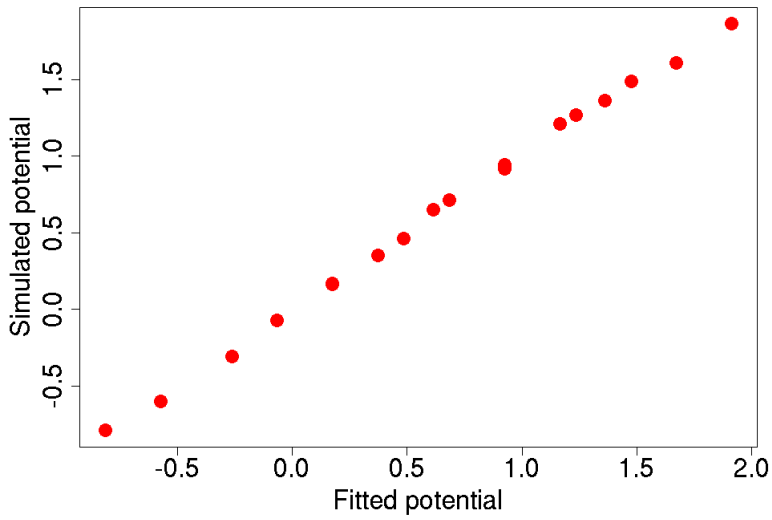

Figure 4.5: Height of the potential structure modeled by function 4.1.

To demonstrate the exact influence of the structure, two extreme cases were selected - small Debye length (n = 1×10^{19} m^{-3}, T_i = 40 eV) and large Debye length (n = 2×10^{18} m^{-3}, T_i = 100 eV). Side-by-side comparison of the potential distribution (Fig. 4.6) and flux profiles (Fig. 4.7) shows that the transport of plasma inside the gap can be in two different regimes. In case of large Debye length, there is almost no potential structure and so the decays are exponential. The fraction of repelled ions is 60%, 3% hit the right tile and 37% the left tile. In case of small Debye length the potential structure is

well developed and the transport barrier inside the gap gives rise to plateau region near the entrance. Fraction of repelled ions is only 23%, 5% reach the right tile and 72% the left tile. The transition between the 2 regimes appears to be smooth.

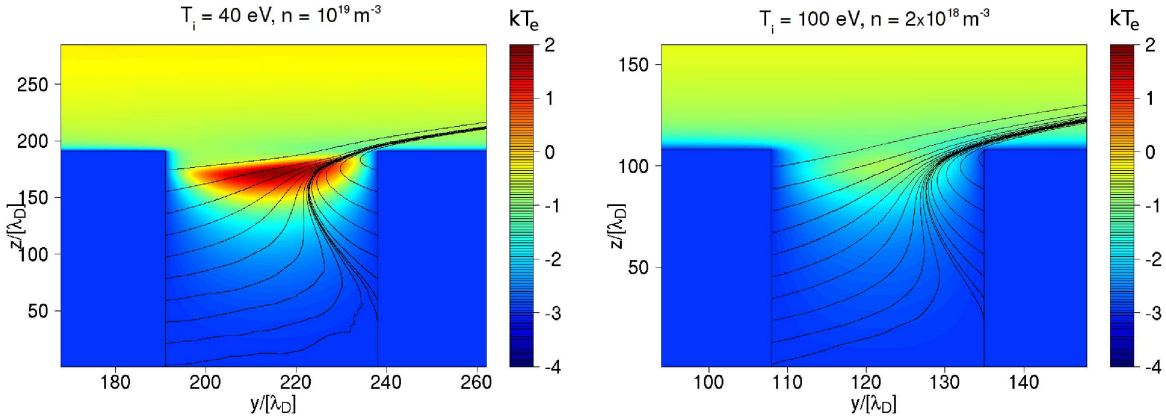

Figure 4.6: Potential distributions for the extreme cases.

4.1.3 Fitting of the particle fluxes

In order to facilitate implementation of the particle fluxes into the 3DGAP code, the flux curves had to be represented by analytical functions. For this purpose, a fully automatic fitting procedure was developed. The flux curve is split into 2 regions - the decay deep inside the gap (modeled by an exponential) and the main flux, which is fitted by a parabola. This fitting scheme proved to be quite robust and was capable of approximating the fluxes for all studied cases and for both tiles within the precision of 10%. An example of such fit is shown in Fig. 4.8.

4.1.4 Gap size study

In order to optimize the choice of the gap size, a series of simulations was made for gaps of 0.25, 0.5, 1.0, 1.5 and 2.0 millimeters. The results show that for wider gaps, the plasma penetrates deeper and the maximum flux increases (see Fig. 4.9). It also shows the build-up of potential structure (in wide gaps ions are more like to reach the shadowed region) and a change in flux curve shape, which confirms that the potential structure works as a

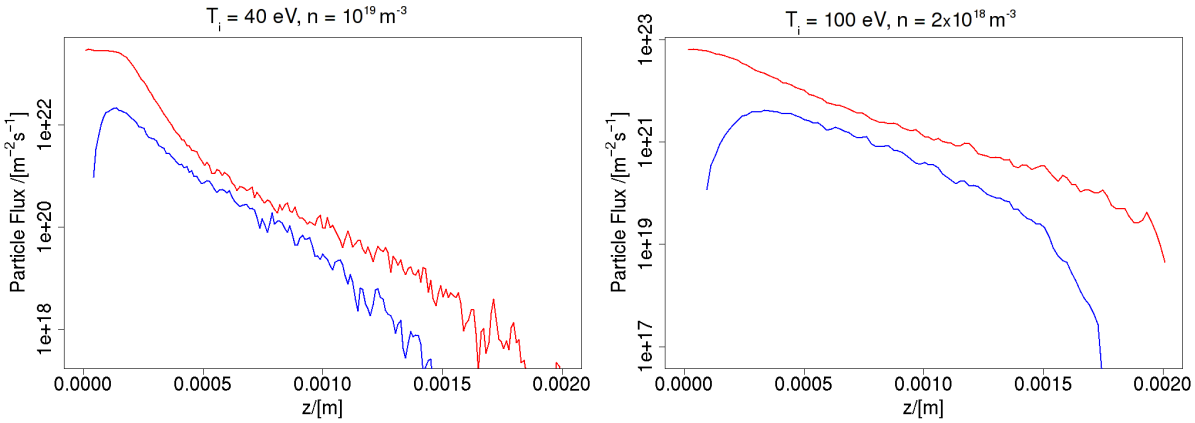

Figure 4.7: Ion flux distributions along the gap for the extreme cases. Left tile in red, right tile in blue.

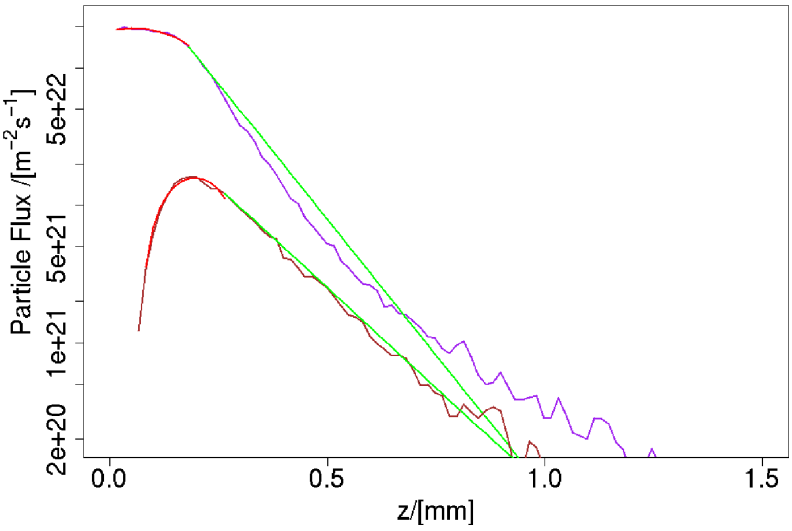

Figure 4.8: Fitting of the particle fluxes for the standard case. Red curves are parabolic fits, green curves exponential fits.

transport barrier. The dependence of the height of the potential structure on the gap size is plotted in Fig. 4.10. Clearly, for all cases except the 0.25 mm gap, the transport is in the potential-dominated regime. The fraction of repelled particles slightly increases with gap size (from 18% up to 35%), which is an unexpected result. Apparently there are 2 mechanisms for ion bouncing, which complement each other. One is due to the electric fields in the sheath and the other is related to the potential structure.

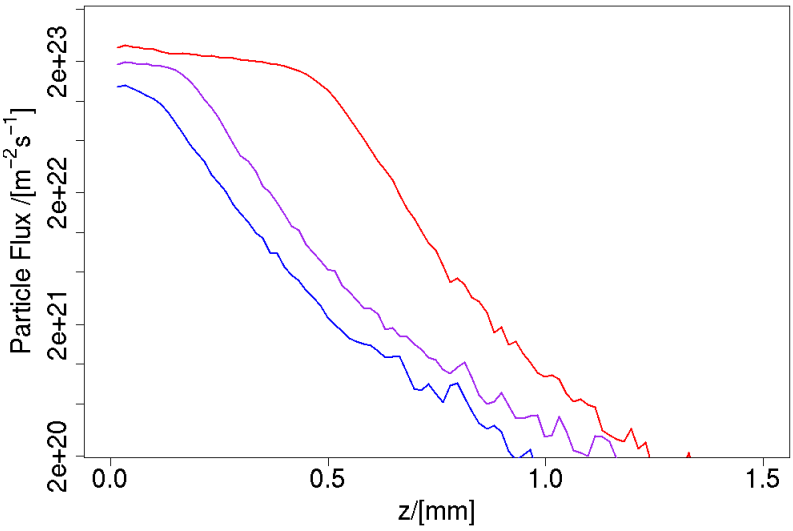

Figure 4.9: Particle fluxes on plasma-wetted gap side for gaps of 0.25 mm (blue), 0.5 mm (purple),1.5 mm (red).

4.1.5 Carbon transport

The SPICE2 code allows simulations of plasma impurities. The most common impurity in TEXTOR is carbon C^{3+}. Carbon ions coming from plasma accelerate through the sheath and due to their charge the impact energy is much higher than in the case of deuterium, causing intensive sputtering. It is therefore useful to know how deep can such ions penetrate into the gap and what is their repelled fraction. However, the important properties of carbon such as temperature and velocity distribution are unknown from experiment and have to be estimated. The presented results are therefore only preliminary. We have assumed thermalized carbon with the same velocity

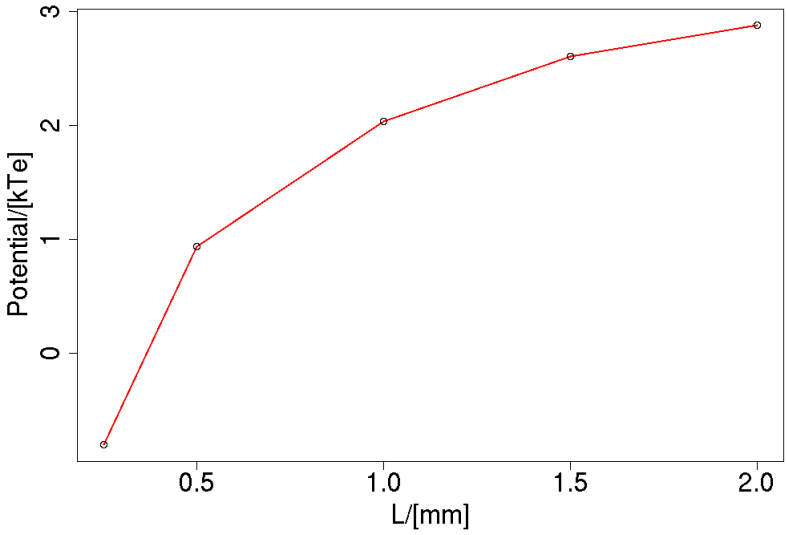

Figure 4.10: Height of the potential structure depending on the gap width L.

distribution as deuterium. A simulation was performed with the standard plasma conditions with 3% of C^{3+}. The carbon flux curves are shown in Fig. 4.11.

Carbon particle flux is localized near the entrance of the gap, it only penetrates 0.5 mm inside. This is contradictory to assumptions used in the 3DGAP code (which assumes the carbon penetration to be the same as that of deuterium), however more studies are needed to verify this difference. The repelled fraction is 70%, which is higher than in case of deuterium. Both of these results are a consequence of smaller Larmor radius.

4.1.6 Shaped gaps

Shaping of the gaps is a way to reduce unfavorable effects of castellation - elevated heat loads at the tile edges and penetration of plasma into the gaps. Experiment with shaped poloidal gaps has been performed at TEXTOR. The geometry of the shaping is shown in Fig. 4.1. The shift between tiles is 3 mm, one surface is inclined at $\alpha = 20°$, which makes it parallel to the magnetic field and the other one at $\beta = 18.5°$. In order to improve the understanding of transport processes in shaped gaps, the same parameter study was performed as in the case of non-shaped gaps. Inclined surfaces

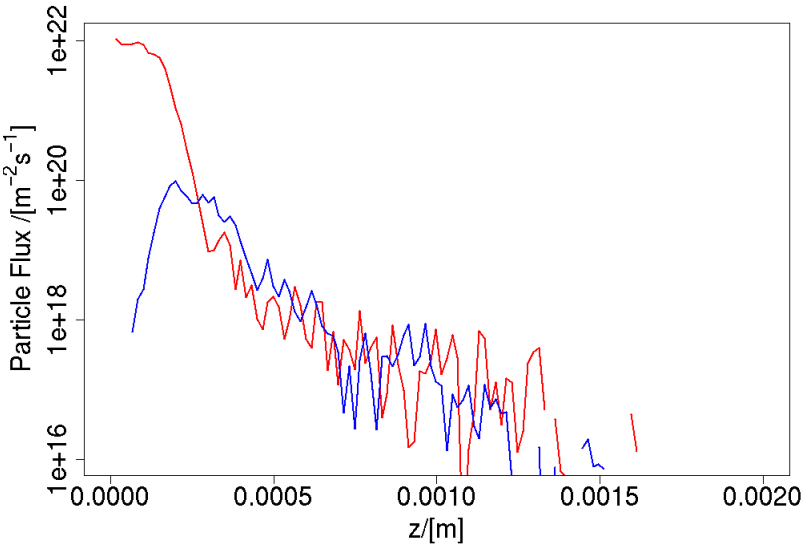

Figure 4.11: Carbon particle flux for 3% of C^{3+}, standard plasma conditions. Left tile in red, right tile in blue.

in SPICE2 code are approximated by staircase (the space is discretized into cells of size of λ_D). This requires special care when extracting flux to such surfaces. Since detailed spatial resolution is not needed for fitting, the flux has been averaged over each step of the staircase.

The potential distribution in the standard case is shown in Fig. 4.12. Due to large shadowed region, the potential structure is well-developed, exceeding 3 kT_e in its maximum, which is much more than in the case of non-shaped gaps. This represents a significant barrier for ions, which results in reduced transport inside the gap. This is visible in the distribution of particle fluxes along the right tile inside the gap (Fig. 4.13). The flux drops to negligible levels on the first 2 millimeters of the tile, which means that there is no plasma at all inside the gap on neither side. This demonstrates the effectivity of shaping, in case of non-shaped gaps the plasma penetration was typically 1.0 mm. The deposition inside shaped gaps is therefore not directly influenced by particles coming from plasma.

However, shaping is only possible for poloidal gaps, toroidal gaps can still exhibit intensive plasma penetration. The particle fluxes on the top surfaces and along the right tile have been fitted in the same way as for non-shaped gaps, in order to implement them in the 3DGAP code.

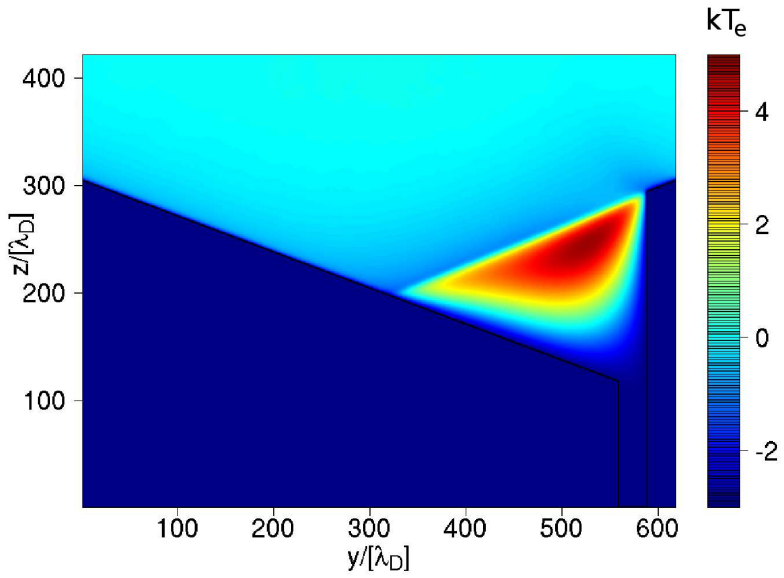

Figure 4.12: Potential distribution for standard plasma conditions, shaped gap.

4.2 Coupled simulations

In the previous section, the parameter study was performed in order to understand the plasma behavior in the vicinity of gaps. As an important outcome, a database of particle flux distributions for range of plasma conditions typical for the TEXTOR tokamak was created. This allows implementing realistic plasma fluxes in the impurity transport simulations performed by the 3DGAP code.

4.2.1 3DGAP code

The 3DGAP code has been developed by D. Matveev [10] at Forschungszentrum Jülich to model impurity transport and deposition inside tile gaps. It is a 3D Monte-Carlo code, which allows tracking of neutral and charged test particles. The particles are emitted by sources inside and outside the gap, which represent the physical processes like reflection, erosion, physical and chemical sputtering. The simulation is divided into timesteps of typical duration of 0.1s. During each timestep, a number of test particles is emitted from the sources and traced until they hit the tiles or leave the simulation volume through the gap entrance. At the end of each timestep, the deposition

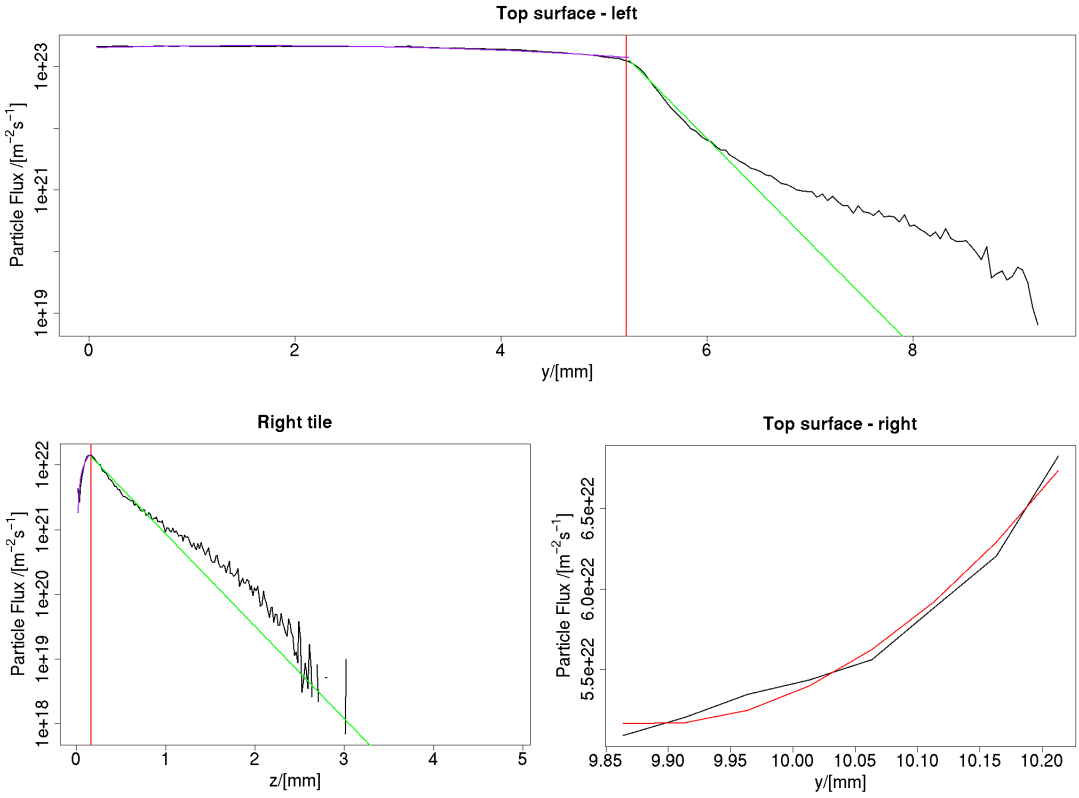

Figure 4.13: Particle flux fitting of shaped gap for both top surfaces and on right tile along the gap.

data are updated for the next iteration. The code implements homogeneous material mixing model (HMM) inside the surface to assess the build-up of mixed layers. This model distinguishes the surface layer (interaction layer) with homogeneous distribution of species, which takes part in all interaction processes, and the bulk, which does not contribute to the interactions but works as a particle reservoir. Number of particles in the interaction layer is kept constant, and the excess/lack of particles is compensated by moving particles into/from the bulk. Accordingly, the processes of erosion depend on the concentrations of species in the interaction layer. The 3DGAP code also uses several modules and databases of the ERO [26] code, such as the neutral collisions model and electron impact ionization rates.

A recent dedicated experiment with ITER-like castellation geometry performed at TEXTOR tokamak [27] has been selected for the code benchmarking (0.5mm wide gaps). It has been demonstrated that formation of low sticking hydrocarbon radicals as a result of chemical erosion is responsible for deposition of carbon deep inside the gap. The chemical erosion yield Y_{chem}, which represents the number of extracted carbon atoms per incident D atom is one of the key parameters influencing the simulations. Up to now, only partial agreement with experiment has been achieved. Although, modelling results agree with experimental data for side surfaces of the gap, the carbon deposition at the bottom of the gap appears to be much higher in experiment than predicted by modeling.

The particle sources of deuterium and carbon neutrals in 3DGAP depend on the ion fluxes from plasma. These fluxes have been estimated so far using plasma parameters from experiment, and have large degree of uncertainty. It has been also assumed that the plasma flux is homogeneously distributed over the first 0.5mm of plasma-open side near the gap entrance. In order to restrict the range of parameters, which govern the simulation, a realistic D^+ flux and its distribution over the gap surfaces is needed. In the frame of this work, it will be calculated using the SPICE2 code. Additionally, the plasma background and the sheath electric field provided by SPICE2 will be applied in 3DGAP in order to study the effect of ionization of particles leaving the gap.

4.2.2 Results of coupled simulations

Simulations in 3DGAP require knowledge of a number of parameters, which are only partially provided by experiment. These are mainly the reflection probabilities for carbon, deuterium and hydrocarbons (R_C, R_D and $R_{C_xD_y}$ respectively) and the chemical erosion yield Y_{chem}. The simulation strategy therefore consists of iterative attempts to match the experimental deposition

profiles. Usually a satisfactory agreement is found for a single set of parameters. Previously, the simulations were done assuming homogeneous ion flux coming from plasma on the first 0.5 mm of the gap (on the plasma-wetted side). The purpose of coupled simulations was to see if these parameters change when the realistic particle flux distribution is included in the calculations.

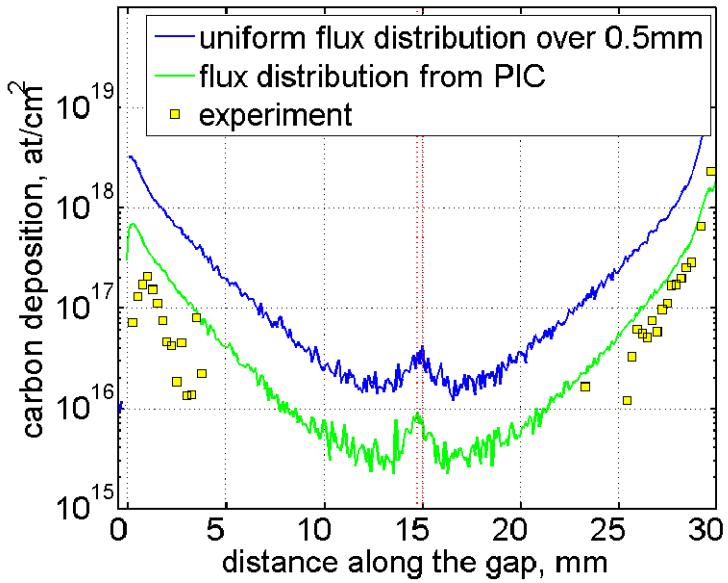

Figure 4.14: Comparison of the deposition calculated by 3DGAP code with and without the particle flux distributions from SPICE2 code for standard plasma conditions, non-shaped gap.

3DGAP simulations without the fluxes from SPICE2 code made best match with experimental results for parameters $R_C = 0.6$, $R_D = 0.7$, $R_{C_xD_y} = 0.9$ and $Y_{chem} = 2\%$. When the SPICE2 fluxes were introduced, the shape of carbon deposition profile did not change and still agreed with experiment for the same parameters. This is mainly due to the fast decay of the fluxes in the shadowed region. However, the total amount of particles entering the gap is different. Certain part of the ions (typically 20%) is repelled by the potential structure and does not enter the gap. The deposition profiles are shown in Fig. 4.14. Note that the deposition at the bottom was omitted from the plot. This unexpectedly high deposition has never been reproduced by 3DGAP modeling. More importantly it has not been observed in other similar experiments. It may be a consequence of disruptions, which occurred

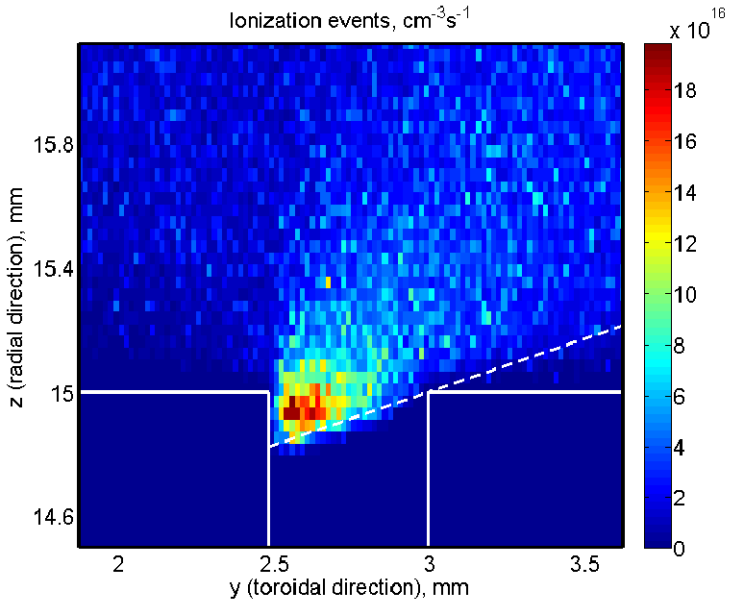

Figure 4.15: Ionization events for standard case, non-shaped gap.

during the experimental campain. Fig. 4.15 shows the 2D map of ionization events due to electron impact on deuterium calculated by the 3DGAP code. All the ionization takes place outside the shadowed region.

Results for shaped gaps (Fig. 4.16) are similar to the non-shaped ones. Introduction of the SPICE2 fluxes does not change the character of carbon deposition, only the absolute values are scaled. Since the plasma does not penetrate into the gap itself, there is no ionization of the neutral, as shown in Fig. 4.17.

The results of ionization distributions have important impact on the transport mechanisms inside the gap. Neutral atoms and molecules can be released from the tiles by refection or erosion inside the gap and move freely. Should they be ionized inside the gap, the potential structure near the entrance could work as a transport barrier and prevent them from escaping to the main plasma. This could lead to higher deposition, since the particles would be in fact trapped inside the gap. Coupled simulations clearly show that this is not the case.

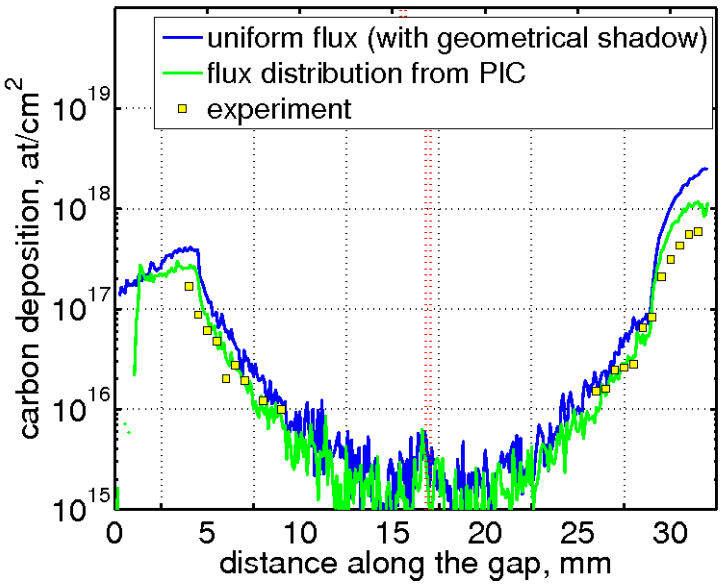

Figure 4.16: Comparison of carbon deposition calculated by 3DGAP code with and without the particle flux distributions from SPICE2 code for standard plasma conditions, shaped gap.

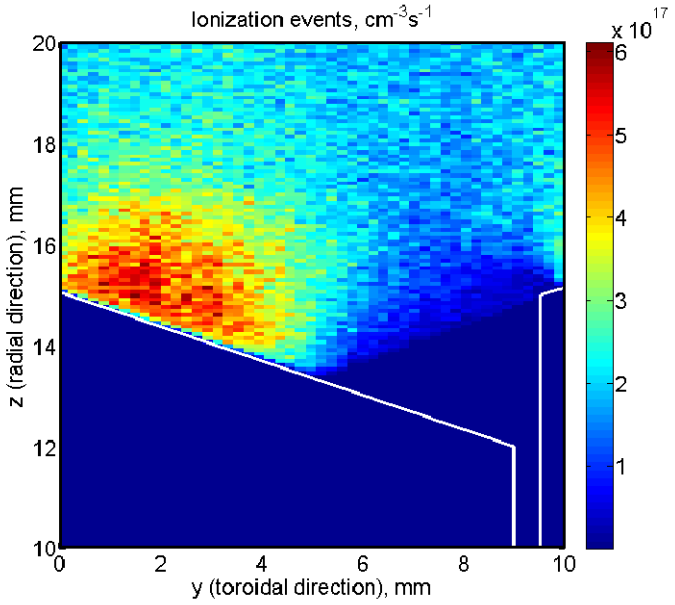

Figure 4.17: Ionization events of deuterium for standard case, shaped gap.

Chapter 5

Fluid modeling

5.1 Introduction

Fluid modelling is one of the commonly used ways of simulating the SOL in tokamaks. Unlike kinetic modelling, which deals with individual particles, fluid modelling works with continuous quantities - density, pressure, temperature etc. The simulation iterative scheme consists of simultaneous solution of diffusion-type equations for key plasma parameters. Similarly to the Particle-In-Cell technique, the space is discretized by a mesh but the size of the cells here is much larger, typically in order of centimeters. This allows simulations of the entire tokamak plasma, which would be impossible in kinetic modelling due to computational constraints. However, fluid modelling is valid only when a number of assumptions is fullfiled - the main ones are quasineutrality of plasma and Maxwellian distribution of velocities. Whether or not such assumptions are always valid in the scrape-off layer plasmas is a subject of ongoing discussion. However, fluid codes have been used for modelling of tokamak plasmas for decades and they represent a useful tool when trying to understand hot plasma behavior. The objective of this work is to port one of such codes, B2SOLPS, to the geometry of COMPASS tokamak.

5.2 B2SOLPS code

The B2SOLPS transport fluid code [28][14][29] is a commonly-used package of codes used to simulate plasma on a number of tokamaks including JET, Asdex-Upgrade and MAST. Like other fluid codes it is based on conjugate solution of fluid transport equations equivalent to Braginskii [30] scheme. The code takes into account drifts and currents. It is capable of simulating H-mode discharges if the profile of diffusion coefficient includes transport

barrier (sudden drop of diffusivity over a short radial interval). However, it only operates with time-averaged physical quantities, so it is not capable of reproducing ELMy behavior.

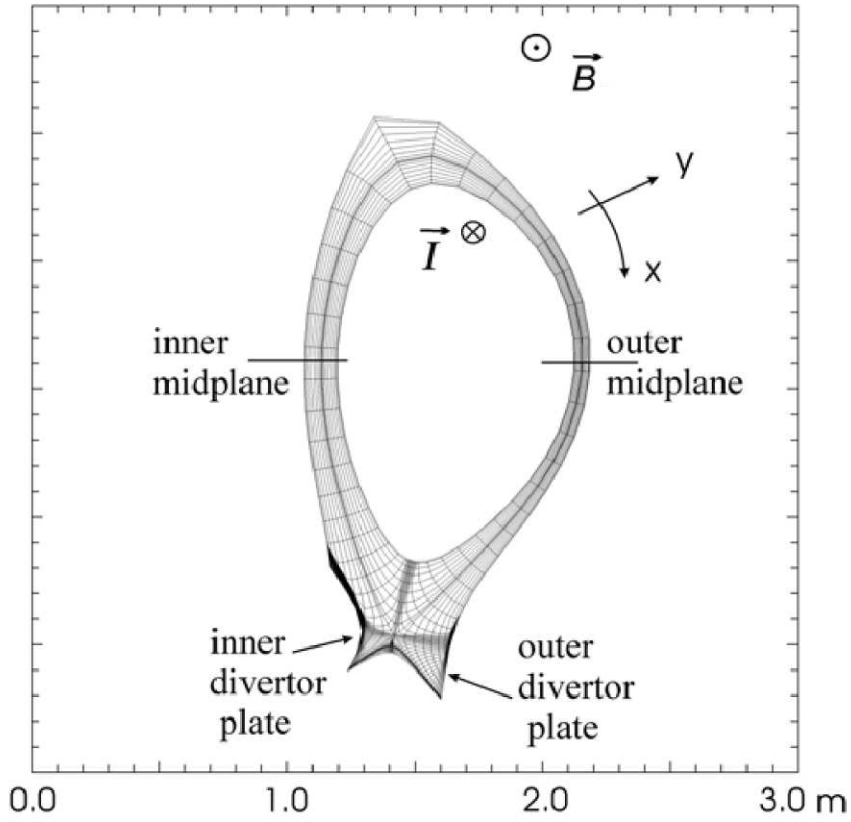

Figure 5.1: B2SOLPS coordinate system and a mesh for the Asdex-Upgrade tokamak.

B2SOLPS code is working in curvilinear geometry, as shown in Fig 5.1. The suitable mesh is a key to successful calculations. In general, the cells of the mesh follow the flux surfaces provided by the EFIT code (based on experimental data) from a tokamak. Since there is no experimental equilibrium available from COMPASS, we have used equilibrium calculated by ACCOME code [31], which has been modified to suit better the calculation scheme (the triangularity was reduced to increase SOL width). Such equilibrium may seem somehow artificial but the purpose of simulations was not to reproduce a real COMPASS discharge but to identify issues concerning calculations of COMPASS-like geometry.

5.3 Simulation parameters

The COMPASS tokamak has been successfully reinstalled in Prague and achieved first plasma on the 9.12. 2008. However, most of the diagnostics are still under development so there is very little information about the plasma characteristics. COMPASS is now operated under rather different conditions comparing to previous operation in Culham. There the plasma was heated by ECRH antenna, which caused the electron temperature to be significantly higher than that of ions. For this reason within this thesis it was not possible to use existing experimental results when setting up the B2SOLPS simulations. Instead results of modeling were used. The diffusion coefficient was estimated to $D_\perp = 1\ m^2/s$ and heat conductivity $\chi_\perp = \frac{1}{4}D_\perp$. The plasma temperature at the inner boundary of simulated region (approximately 3 cm inside the separatrix) was estimated to 100 - 300 eV, density between $2 \times 10^{19}\ m^{-3}$ and $6 \times 10^{19}\ m^{-3}$. A parameter study in n and T was performed to find operation window, where the B2SOLPS converges.

5.4 Results of simulations

The schedule of simulations was the following - first simulations within the range of estimated plasma parameters without the $E \times B$ drift were performed to get initial insight in the plasma behavior. For this the timestep of 10^{-6}s was sufficient. Then, the influence of drift was introduced by subsequent increase of its weight from 0.0 to 1.0 by steps of 0.1 with timestep reduced to 10^{-7}s or even 10^{-8}s. The inclusion of $E \times B$ has in general negative impact on the convergence of the simulation, however it makes the results more realistic - especially the radial profile of potential. It turned out that the code converges better for low-performance plasma. The best results were obtained for n = $3 \times 10^{19}\ m^{-3}$ and T = 100 eV. In this case we have been able to reach convergence at full value of the ExB drift. 2D map of electron temperature (Fig. 5.2) and radial profile ion density (Fig. 5.3) show standard plasma behavior with well-pronounced influence of separatrix.

In order to partially validate the results of simulations, the radial electric field profile was compared with neoclassical calculation

$$E^{NEO} = \frac{T_i}{e}\left(\frac{1}{h_y}\frac{dlnn}{dy} + k^T\frac{1}{h_y}\frac{dlnT_i}{dy}\right) - b_x\frac{\oint\sqrt{g}V_{||}Bdx}{\oint\sqrt{g}dx}, \qquad (5.1)$$

where h_y is the metric coefficient of the curvilinear mesh, $\sqrt{g} = h_x h_y h_z$, and k^T is a coefficient chosen according to [32]. The result is shown in Fig.5.4. The although the trends of the curves are similar, it is far from an agreement.

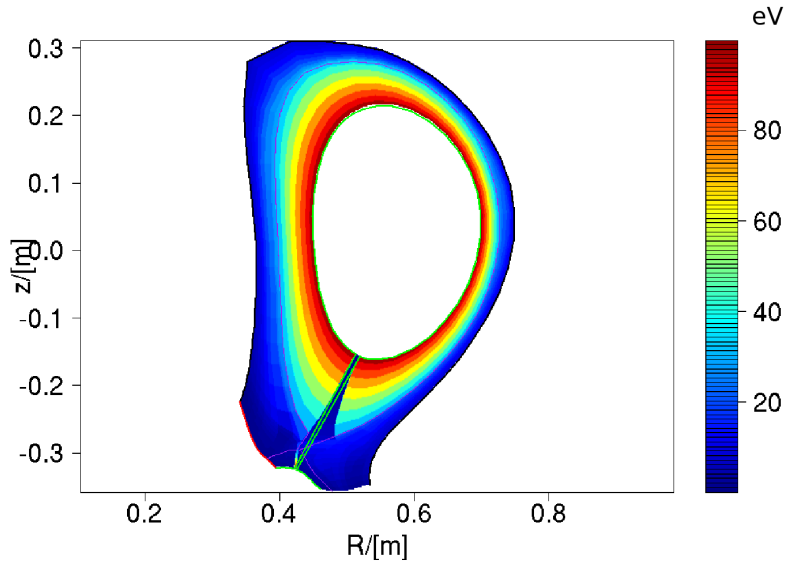

Figure 5.2: 2D poloidal map of the electron temperature.

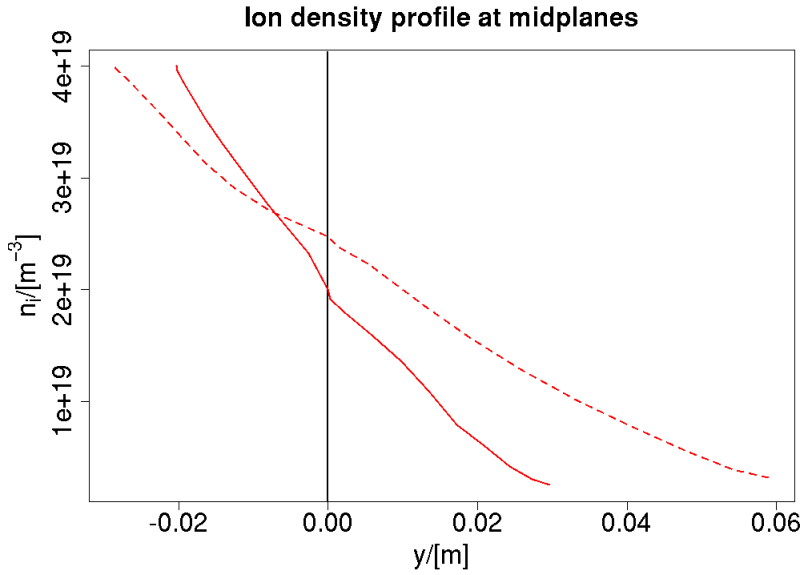

Figure 5.3: Radial profile of ion density at the outer (full) and inner (dashed) midplane. Zero in the y coordinate denotes separatrix.

There are more possible reasons for this discrepancy. It is not to be expected to reach perfect match between the neoclassical model and the simulation. The model is much more simple and neglect certain aspects of the plasma behavior. Second is the absence of viscosity associated with the parallel heat flux, which has not been taken into account in the simulations yet. This topic will be a further subject of development.

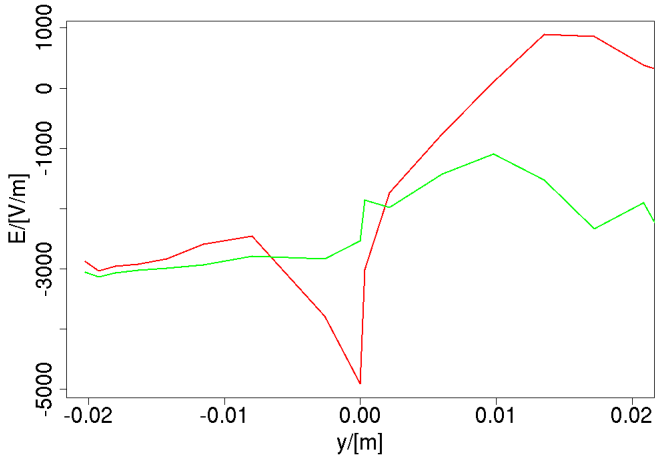

Figure 5.4: Radial profile of electric field at the outer midplane, B2SOLPS simulation (red line) in comparison with neoclassical calculation. Zero in the y coordinate denotes separatrix.

5.5 Outlook

The presented results show that B2SOLPS is capable of simulating the SOL of COMPASS. However, much work is still left to be done in order to reproduce real conditions in specific discharges. A toolchain for facilitating the semi-automatic mesh generation needs to be developed, some of the key parameters (diffusivity, pumping rate) have to be measured, etc. The future plan is to use the code to provide detailed information about profiles of key plasma quantities for specific discharges in order to compare them with experimental data. One such opportunity will be a foreseen experimental campaign with reciprocating ball-pen probe, which should measure the radial electric field profile.

Chapter 6

Summary and Outlook

The plasma behavior in the vicinity of castellated surfaces in tokamaks is a subject of intensive research, mainly because of safety implications for ITER and future fusion reactors. The SPICE2 code is capable of calculating ion flux distribution inside the tile gaps. The main objective of this thesis was to calculate such fluxes for typical plasma conditions in the SOL of the TEXTOR tokamak, which can be subsequently used in the impurity transport code 3DGAP.

In order to complete tasks of this work, the SPICE2 code had to be reviewed and extended to allow simulations of inclined surfaces. New diagnostics for measuring particle flux onto solid surfaces were implemented.

A parameter study of plasma behavior in vicinity of TEXTOR test limiter tile gaps was performed. Two transport regimes, *potential-driven* and *geometry-driven*, were identified and the importance of the potential structure near the gap entrance was demonstrated. The dependence of the potential structure height on the Debye length was discovered and fitting function found. Database of more than 50 scenarios with varying plasma conditions was created for use in future studies. In most cases, the plasma penetrates approximately 1.0 millimeter into the gap (double of the gap width) and the ion fluxes are distributed on both sides of the gap. For the standard studied case, 72% percent of the flux hits the plasma-opened side of the gap, 5% to the shadowed tile and 23% is repelled by the potential structure. Study of the influence of gap size on transport inside the gaps was performed. The results show that gaps wider than 0.25 mm are governed by the *potential-driven* regime. A testing simulation of C^{3+} impurity transport in the gap was fulfilled, confirming previous assumptions on shallow carbon penetration used in impurity transport simulations. Generic fitting procedure consisting of partial parabolic and partial exponential fit for the ion flux distribution along the gap was developed, which allowed integration of such fluxes in

the 3DGAP code. New simulations in 3DGAP code with output of SPICE2 runs were compared with previous results and the importance of repelled flux fraction demonstrated. The results show that the ionization inside the gap is negligible and can be omitted from the impurity transport model.

Shaped poloidal gaps were studied for typical TEXTOR conditions. In all studied cases the plasma does not penetrate at all into the gap. Fitting of particle loads on inclined surfaces was done and used in the 3DGAP code. The transport regime for shaped gaps was identified as potential-driven. Simulations of the SOL of the COMPASS tokamak were performed by using the B2SOLPS code. Toolchains facilitating simulation control and data processing were developed. The convergence window of the code for COMPASS geometry was found, and simulation with drifts were accomplished. Comparison of radial electric field profile with neoclassical model was performed with low level of agreement. In the frame of this thesis two important collaboration links were established. The first one connects Forschungszentrum Jülich and IPP Prague in joint effort to explain plasma behavior in gaps of castellated plasma facing components, which is an important issue for the ITER device and future fusion reactors. Coupled simulations of SPICE2 and EDGE3D should help in better understating of layer formation inside the gaps.

The second collaboration links research group at the State Polytechnical University of St. Petersburg with IPP in Prague. Simulations of the COMPASS tokamak by using the B2SOLPS code will be an useful source of information about the plasma behavior in scrape-off layer. Comparison of modeling with experimental data from advanced probes is foreseen.

Acknowledgments

This work is a result of intensive collaboration between Forschungszentrum Jülich, Institute of Plasma Physics CAS CR, v.v.i., State Polytechnical University of St. Petersburg and CEA Cadarache. It would be impossible to accomplish without devoted help of many people.

I would like to thank my thesis promoters Prof. Guido van Oost, Prof. Geérad Bonhomme and Prof. Michael Tendler for their help with the arrangement of thesis topic.

I express my gratitude to Dr. Andreas Kirschner for continuous encouragement and guidance during the work on this diploma and valuable recommendations concerning the text of the thesis.

Understanding of the TEXTOR test limiter experiments and modelling would be impossible without discussions with Dr. Andrey Litnovsky and Dr. Dmitry Borodin, as well as with Dmitry Matveev who spent lots of time explaining to me the functionality of the 3DGAP code and running impurity transport simulations.

I would like to thank Prof. Vladimir Rozhansky, Dr. Elisa Kaveeva, Pasha Molchanov, Dr. Ilya Senichenkov and other members of the modelling group in St. Petersburg for providing me insight into the fluid modeling and functionality of the B2SOLPS code.

I am grateful to Dr. Renaud Dejarnac and Dr. James P. Gunn, coauthors of the SPICE2 code, for helpful discussions concerning extension of the SPICE2 code and problematics of the plasma sheath.

The B2SOLPS simulations could only be performed thanks to great support of Dr. Jan Horacek, Josef Havlicek, Pavel Cahyna, Michal Stransky and Jara Cimrman, who provided me with estimated COMPASS tokamak parameters.

I would like to thank Natasha Bathauer for valuable inspiration concerning the potential structures.

Bibliography

[1] J. Ongena and G. Van Oost. *Trans. Fusion Sc. Tech.*, (53), 2008.

[2] J.A.Wesson. *Tokamaks*. Oxford University Press, 1987.

[3] http://www.iter.org. Iter project.

[4] M. J. Rubel et al. *Phys. Scr.*, (112-117), 2004.

[5] C.H. Skinner. *Nucl. Fusion*, (271), 1999.

[6] R. Dux et al. *J. of Nucl. Mat*, (390-391), 2009.

[7] J. Roth et al. *J. of Nucl. Mat.*, (390-391), 2009.

[8] A. Litnovsky et al. *J. of Nucl. Mat*, (390-391), 2009.

[9] A. Litnovsky et al. *J. of Nucl. Mat.*, (809-812), 2009.

[10] D. Matveev. *Modeling of material deposition in the gaps of castellated surfaces in fusion experiments*. diploma thesis, 2009.

[11] J. Stockel R. Dejarnac, M. Komm and R. Panek. *J. of Nucl. Mat.*, (382), 2008.

[12] V. Naulin. *J. of Nucl. Mat*, (363-365), 2007.

[13] R. Chodura. *Phys. Fluids*, 25:1628, 1982.

[14] V. Rozhanski. *Phys. Control. Fus.*, (46), 2004.

[15] C.K. Birdsall and A.B. Langdon. *Plasma Physics via Computer Simulation*. McGraw-Hill, New York, 1985.

[16] Y. Idomura et al. *Comp. Phys. Comm.*, (179), 2008.

[17] J.P. Gunn R. Panek R. Dejarnac, M. Komm. *J. of Nucl. Mat.*, (390-391), 2009.

[18] M. Komm J.-Y. Pascal E. Gauthier M. Kocan, J. P. Gunn and G. Bonhomme. *Rev. Sci. Instrum.*, (79), 2009.

[19] J.P. Gunn. *J. Nuclear Mater*, 337-339:310, 2005.

[20] O. Buneman. *J. Comput. Phys*, 1:517, 1967.

[21] H. William et al. *Numerical Recipes in Fortran*. Cambridge University Press.

[22] http://www.cise.ufl.edu/research/sparse/umfpack/. Umfpack library.

[23] http://www.tacc.utexas.edu/resources/software/#blas. Gotoblas library.

[24] http://www.open mpi.org. Openmpi library.

[25] http://spice2.sourceforge.net. Spice2 homepage.

[26] A. Kirschner et al.1. *J. of Nucl. Mat.*, (290-293), 2001.

[27] A. Litnovsky et al. *Phys. Scr.*, (45-49), 2007.

[28] V. Rozhanski et. al. *J. of Nucl. Mat.*, (390-391), 2009.

[29] V. Rozhanski. *Phys. Control. Fus.*, (46), 2005.

[30] Braginskii S.I. *Reviews of Plasma Physics*, (1), 1965.

[31] M. Azumi K. Tani and R. S. Devoto. *J. of Comp. Phys.*, (98), 1992.

[32] Hinton F.L. and Hazeltine R.D. *Rev. Mod. Phys*, (48), 1976.

Declaration in lieu of oath

Herewith I declare in lieu of oath that I have prepared this thesis exclusively with the help of my scientific teachers and the means quoted by them.

Jülich, the June 25, 2009

_____

Michael Komm